

# A computational study of the EN 1078 impact test for bicycle helmets using a realistic subject-specific finite element head model

**Sandberg, Michael; Tse, Kwong Ming; Tan, Long Bin; Lee, Heow Pueh**

*Published in:*
Computer Methods in Biomechanics and Biomedical Engineering

*Link to article, DOI:*
10.1080/10255842.2018.1511775

*Publication date:*
2018

*Document Version*
Peer reviewed version

# A computational study of the EN 1078 impact test for bicycle helmets using a realistic subject-specific finite element head model

Michael Sandberg[1,2*], Kwong Ming Tse[1,3*], Long Bin Tan[1], and Heow Pueh Lee[1]

[1]*Department of Mechanical Engineering, National University of Singapore,*
*9 Engineering Drive 1, Singapore 117576;*

[2]*Department of Mechanical Engineering, Technical University of Denmark,*
*DK-2800 Kgs. Lyngby, Denmark*

[3]*Department of Mechanical and Product Design Engineering, Swinburne University of Technology,*
*Advanced Technologies Centre, John St, Hawthorn, Melbourne, VIC 3122, Australia*

*Corresponding authors:

michaelsandberg@mail.com / misan@mek.dtu.dk (Sandberg, M.)

tsekm.research@yahoo.com / ktse@swin.edu.au (Tse, K.M.)

# A computational study of the EN 1078 impact test for bicycle helmets using a realistic subject-specific finite element head model


## Abstract

In this paper, the authors aim to establish a numerical framework for computational injury assessment of protective headgear subjected to drop tests. The case study is a bicycle helmet considered in a guided free fall impact test in accordance with the EN 1078 standard for certification of bicycle helmets. A finite element model of a bicycle helmet is created based on generic values for material properties and thicknesses of the helmet layup. The helmet model is coupled to an experimentally validated subject-specific finite element head model. This together constitute the numerical framework, which is found to be adequate by verification against other published results. The impact scenario is simulated with and without a bicycle helmet, and it is demonstrated that the helmet reduces peak resultant translational acceleration, von Mises skull stresses, intracranial pressure, and strain in the brain during the impact.



**Keywords:** head injury; bicycle helmet; drop test; biomechanics; crushable foam


## 1 Introduction

With increasing public awareness of health, fitness, and air pollution, cycling is popular as an alternative to the automobile. In countries like the Netherlands and Denmark, there are approximately 5 million and 1 million cyclists, or about 31% and 19% of the respective population, who prefer bicycles for commutation (European Commission, 2011). Nevertheless, cycling has associated safety risks. Cyclists are generally considered vulnerable road users, whereby a minor misjudgement by a vehicle driver can have significant adverse consequences on a cyclist. As opposed to other modes of commutation, cyclists only have their helmets for protection against fatal injuries in collisions. Therefore, it is particularly important

39 that bicycle helmets follow proven design standards.

40 Bicycle helmet standards generally require that the helmet manufacturers test and qualify their
41 products by performing guided free fall drop tests using artificial headforms. Peak headform
42 accelerations obtained in these tests are then compared against the thresholds prescribed in the
43 standards. For instance, in the United States, the Consumer Product Safety Commission
44 (CPSC, 1998) requires the registered headform peak accelerations to be below 300G for both
45 a 2 m drop (pre-collision velocity of 6.3 m/s) on a flat anvil and 1.2 m drop (4.9 m/s) on
46 hemispheric and curbstone anvils. In Europe, Asia, and South America, the acceleration
47 threshold is 250G for both a 1.5 m drop (5.42 m/s) on a flat anvil and a 1.06 m drop (4.57 m/s)
48 on a kerbstone anvil. Other standards include AS/NZS 2063 (Australia), CAN/CSAD1 13.2-M
49 (Canada) and JIS T 8134 (Japan). Readers are referred to HEADS-ITN (2015) for a
50 comprehensive overview of the current helmet standards.

51 There are currently 28 countries with some form of law for bicycle helmet use (ITF, 2017;
52 European Commission, 2015, 2016; Bicycle Helmet Safety Institute, 2017). Moreover,
53 approximately half of the members of the Organisation for Economic Co-operation and
54 Development (OECD), the International Traffic Safety and Data Analysis Group, and the
55 European Union have some form of bicycle helmet legislation. Wearing a helmet while cycling
56 has been proven as an effective way to mitigate head injuries in relation to collisions (bicycle
57 crashes or falls). Using headform impact tests, Cripton et al. (2014) showed that in a collision
58 at 6.3 m/s and 5.42 m/s, severe brain injury is extremely likely to occur, with 99.9% probability
59 based on the head injury criterion (HIC). However, these probabilities were reduced to 30.6%
60 and 9.3% respectively, for the two impact velocities, when a bicycle helmet is worn. A similar
61 study was published by McIntosh et al. (2013), who conducted impact tests with impact speeds
62 of up to 6.9 m/s in several different impact orientations and locations. Here it was concluded

63 that helmet use was the most significant factor in reducing the probability of head injury. The
64 effect has also been documented through epidemiological studies. Olivier and Creighton
65 (2017) recently completed the largest ever systematic review and meta-analysis by collecting
66 data from 40 different studies from USA, Europe, Australia and Asia. With data based on more
67 than 64,000 injured cyclists, it was concluded that "helmet use is associated with odds
68 reductions of 51% for head injury, 69% for serious head injury, 33% for face injury and 65%
69 for fatal head injury".

70 In addition to the aforementioned experimental and retrospective studies, computer
71 simulations, such as the finite element (FE) method, provides an alternative to experimental
72 methods in estimating the biomechanical responses of the human head. For example, the effect
73 of utilising a bicycle helmet has been demonstrated with FE simulations of three different
74 impact scenarios in Fahlsted (2016)'s study. This study showed that the risks of skull fracture
75 and concussion were reduced by up to 98% and 46%, respectively, by wearing a helmet.
76 Computer simulations for design and optimisation of protective headgear is also an active
77 research field. Potentially, with the growing knowledge about head injuries and capabilities of
78 modern computers, the level of protection can be accessed and analysed using FE simulations.
79 For instance, Mills and Gilchrist (2008) employed a validated FE model of a commercially
80 available bicycle helmet to investigate the effect of friction between the helmet shell and road
81 surface on peak head acceleration in oblique impacts. The effect of foam liner material
82 properties has been investigated by Asiminei et al. (2009), who varied both the density and
83 modulus of the protective foam (expanded polystyrene, EPS). Teng et al. (2013) studied the
84 effect of IMPAXX foam on head impact accelerations, as an alternative to the most commonly
85 used foam type in bicycle helmets (EPS). As outlined, previous research has focused primarily
86 on the helmet materials as well as helmet liners, but limited attention has been paid on head
87 injury assessment. Moreover, many of these computational studies have used oversimplified

FE head models or artificial headforms for the head impact analyses which neither provide insights to the injury mechanics within the brain nor detail the brain regions which could be most affected by the impact.

The current study employs an anatomically detailed and experimentally verified subject-specific head model to simulate the particular impact prescribed by the helmet standard EN 1078 for Europe, Asia, and South America. This computational approach does not only provide an alternative to experimental helmeted drop tests used in bicycle helmet test standards, but also allows injury assessment and evaluation of the intracranial biomechanical injury metrics, such as intracranial pressure (ICP) and strains, which cannot be determined using the headform or simplified FE head models, in these dynamic events. Finally, this study also investigates the effectiveness of a bicycle helmet in protecting our heads.

## 2 Methods and materials

### *2.1 Head model*

Geometrical information of the human skull and brain were obtained from high resolution axial computed tomography (CT) and magnetic resonance imaging (MRI) images of a 51-year-old Caucasian male subject respectively. These medical images were imported into Mimics v13.0-v14.0 (Materialise, Leuven, Belgium) for the segmentation and reconstruction of the FE human head model, which comprises the skeletal skull, nasal septal cartilage, nasal lateral cartilage, with the overlying soft tissue, the cerebrospinal fluid (CSF), the white and grey matters of cerebrum, cerebellum, the ventricular system, the midbrain, the brainstem as well as the air-containing sinuses. Various components of the head model can be seen in Figure 1. All the skeletal tissues such as cartilages and cervical vertebrae were modelled as linear elastic, isotropic materials while the brain tissues were assumed to be linear viscoelastic. The material properties of the various components of the FE head model can be found in Table 1 and Tse et

al. (2014). It should also be noted that the FE head model was validated against the ICP and relative displacement data of three cadaveric experiments (Nahum et al. 1977; Trosseille et al., 1992; Hardy, et al., 2001). More details on the development and validation of the FE head model can be found in Tse et al. (2014).

[Figure 1 around here]

[Figure 2 around here]

[Table 1 around here]

### *2.2 Bicycle helmet model*

The FE model of the bicycle helmet was constructed based on geometry and thicknesses of a generic bicycle helmet layup. In addition, common helmet features such as ventilation holes and retention straps were incorporated in the helmet FE model (Figure 2). The full breakdown of properties and element types are listed in Table 1.

The bicycle helmet consists of five parts: (i) An energy absorbing EPS foam partly covered by (ii) a polycarbonate (PC) shell, with (iii) retention straps, (iv) cushion pads, and (v) a fixture to fit the helmet to the head model. All the components of the bicycle helmet, besides the EPS foam, were considered to be isotropic and linear elastic, and their material properties were taken from previously reported studies (Teng et al., 2013; van den Bosch, 2006; Tan et al., 2012) as shown in Table 1. Following the modelling approaches adopted by Mills and Gilchrist (2008) and Milne et al. (2012, 2014), the crushable foam plasticity model in Abaqus™ (Dassault Systemes, 2013) was used to mimic the EPS foam in this study. In addition, the crushable foam model employed in the study was validated experimentally by Cui et al. (2009) for EPS under impact loads. The constitutive law of this closed cell foam can be described in

three stages:

(i) In the first stage, the material response is linear elastic until the stress state reaches the yield stress.

(ii) In the second stage, the material reaches a plateau level where it continues to deform under an almost constant stress state. This corresponds to the level where most of the energy is absorbed as the foam cells collapse.

(iii) In the final stage, all foam cells have collapsed, and the material response is again linear elastic.

This constitutive law is shown in Figure 3 for the plastic range. According to Dassault Systemes (2013), the yield surface, which is shaped like an ellipse, is described by the following equations (1):

$$\sqrt{\sigma_Y + \alpha(p - p_0)^2} - B = 0, \text{ with } p_0 = \frac{p_c - p_t}{2}, \quad B = \alpha\frac{p_c + p_t}{2}, \quad \alpha = \frac{3k}{(3k_t + k)(3 - k)} \quad (1)$$

where $\sigma_Y$ is the Von-Mises stress, $p$ is the hydrostatic pressure, $p_c$ and $p_t$ are the yield strengths of the material in hydrostatic compression and tension, respectively. $k$ describes the ratio between the initial yield stress in uniaxial compression and initial yield stress in hydrostatic compression, and $k_t$ is the ratio between yield strength in hydrostatic tension and initial yield stress in hydrostatic compression. These values, $k$ and $k_t$, were set to 0.1 and 1.933 (Table 1), respectively, according to Cui et al. (2009), Mills and Gilchrist (2008), and Dassault Systemes (2013).

[Figure 3 around here]

### *2.3 Numerical replication of the EN 1078 standard (contact, boundary conditions, and loading)*

According to the EN 1078 standard, the "to be qualified" helmet equipped with the testing headform undergoes a guided free fall either using a twin wire or monorail test rig onto a flat anvil fixed on a rigid base. In our simulations, an initial velocity of 5.42 m/s corresponding to the final velocity before impact for an object subjected to gravity ($G \equiv 9.81$ m/s$^2$), was applied to the model, before impacting a fixed anvil (Figure 4). All the nodes at the bottom of the anvil were assigned fixed boundary conditions. The entire simulated impact was captured in 6 ms. It should be noted that the pretension in the retention straps of the bicycle helmet was accounted for in an initial step of the simulations prior to the impact, with a preloading of approximately 5 N in each strap according to Mills and Gilchrist (2008).

The interaction between intracranial contents (skull and CSF, CSF and brain tissues as well as self-interaction of intracranial brain tissues) were represented by normal pressure-overclosure and tangential sliding contact definitions, with the coefficient of friction of 0.2 (Kleiven and Hardy, 2002; Willinger et al., 1995; Zhang et al., 2001), while the other extracranial bony and cartilaginous components are fused together. For the interfaces between the helmet and head, and helmet and anvil, contact was defined using a penalty formulation for tangential behaviour with kinetic friction. A kinetic friction coefficient of 0.2 was applied between the head and helmet, and a coefficient of 0.1 between the helmet and anvil in accordance with Milne et al. (2012). Similar to the modelling approaches adopted by Mills and Gilchrist (2008) and Milne et al. (2012, 2014), all the interfaces between different components of the helmet were meshed in such a way that they share common nodes with their adjacent interfaces. This technique is beneficial in terms of reducing computation time and is considered acceptable as no or very little relative motion between individual helmet components is expected. This implies that the

adhesion between components is considered to remain intact during the impact, meaning the collapsible EPS foam is the only helmet component that will absorb energy through irreversible deformation.

### *2.4 Evaluation of head kinematic response and injury metrics*

The kinematic response of the head undergoing the impact was evaluated by its translational accelerations. These were calculated as mean values of the ten nodes nearest the centre of gravity of the head (marked as CG in Figure 1). For assessment of skull and brain injuries, three biomechanical metrics were evaluated to analyse the post-processed transient brain response. *Intracranial Strains:* Maximum principal strains were used as a measure of diffuse axonal injury (DAI). Morrison et al. (2003)'s in vitro tests of living brain tissue showed that a mechanical deformation with a positive principal strain exceeding 0.2 led to cell damage and death, and thus consequently DAI. *Intracranial Pressure (ICP):* ICP has been hypothesised to be one of the most critical biomechanical injury metrics in traumatic brain injury (TBI) since an elevated ICP in head trauma can lead to severe brain damage (Tse et al., 2017). An ICP injury criterion, proposed by Ward et al. (1980) based on combined numerical and experimental investigation of live animals and human cadavers, states that serious or fatal brain injury occurs when the peak ICP exceeds 0.235 MPa, while no or minor brain injury occurs when the ICP is below 0.173 MPa. *Von Mises skull stress:* The critical failure level for the human skull is approximated by a von Mises stress threshold of 75 MPa, which is based on the average of the reported range from McElhaney et al. (1970)'s mechanical experiments conducted on human skull samples.

## 3. Results and discussion

Figure 4 shows the transient accelerations measured at the CG of the head, while Figure 5

illustrates the contour plots of the ICP and principal true strain for the brain, as well as the von Mises stresses of the skull at various time instants during the impact. The peak values are listed in Table 3.

[Figure 4 around here]

[Figure 5 around here]

[Table 3 around here]

### *3.1 Verification of the helmet model and numerical framework*

The peak translational acceleration and impact duration obtained in the current work were benchmarked against Milne et al. (2012)'s and Fahlstedt et al. (2016)'s FE modelling studies, which reported values for the same impact scenario in accordance with the EN 1078 standard. The comparison of the value of these parameters between the present work and the two aforementioned studies is presented in Table 2.

The predicted maximum head acceleration was found to be 223G, which was approximately 28% and 1% higher than the values in Milne et al. (2012)'s and Fahlstedt et al. (2016)'s studies, respectively. As for the impulse duration, our simulation predicted that the impact generated an impulse lasting for 5 ms, while the respective impulse durations in Milne et al. (2012)'s and Fahlstedt et al. (2016)'s simulations were approximately 3 ms and 1 ms longer. The predictions presented in the current study are in good agreement with those values reported by Fahlstedt et al. (2016), even though the peak resultant translational acceleration appears to be overestimated and the impact duration to be underestimated when compared to Milne et al. (2012)'s simulations. These slight differences or discrepancy with Milne et al. (2012)'s study are justifiable due to the different head masses used in these simulations. As shown in Table 2, the

heavier head model used in Milne et al. (2012)'s simulation is expected to result in a more gradual velocity reversal, and thus a lower acceleration due to mass inertia effect. Moreover, our predicted peak head acceleration was also found to be within the 250 G threshold given by EN 1078 standard for direct impact, which implied that the helmet model adequately exemplifies a general bicycle helmet designed according to the EN 1078 standard.

[Table 2 around here]

### *3.2 Injury assessment using biomechanical metrics*

A peak in von Mises skull stress of 85 MPa was obtained at the impact site, shortly after the impact, as shown in Figure 5 and Table 3. This level is above the 75 MPa criterion based on McElhaney et al. (1970), which implies that the impact will result in a skull fracture. When wearing a helmet, the peak von Mises skull stress was reduced to approximately 10 MPa, which corresponds to a reduction of 88%. As this level was well below the failure limit of 75 MPa, this demonstrates that the bicycle helmet is effective in preventing skull fracture for this particular impact condition.

The maximum principal true strain of the brain occurred after the peak in von Mises stress of the skull, due to a natural delay for the motion of the softer viscoelastic brain. The region near the impact zone at the parietal skull bone experienced relative high strains of about 0.8, which was reduced to 0.7 (-13%) by equipping with a helmet. As shown in Figure 5, there were large areas of the brain exceeding Morrison et al. (2003)'s strain injury threshold of 0.2 during the simulated impact duration. This indicates that there is a significant risk of DAI in both impact scenarios, which is however reduced when a helmet is worn as the strain levels are lower.

The intracranial pressure (ICP) response behaved similarly as the brain principal strains. The maximum positive ICP, at 0.65 MPa, was observed in regions close to the impact zone mainly

246 in the grey matter, which was reduced to 0.45 MPa (31%) when a helmet was helmet worn.
247 Both impacts resulted in values that exceeded Ward et al. (1980) ICP threshold of 0.235 MPa,
248 but again a significant reduction was observed when the head model was equipped with the
249 helmet.

250 ***3.3 Limitations***

251 A key limitation of this study was that the intracranial transient responses, which are the basis
252 for injury assessment using the proposed injury metrics, are not only dependent on the physical
253 parameters employed, but also the interaction properties and constraints enforced in the model.
254 As it appears in Figure 5, relative deformation occurred between the intracranial components
255 of the head. In particular, intermittent gaps develop in interfaces between the skull and CSF,
256 and the CSF and white matter during the impact. These are the potential locations for negative
257 ICP which could also be an important biomechanical injury metric, but could also be caused
258 by limitations of the model.

259 The pulsatile cerebrospinal fluid (CSF) was assumed linear elastic for the head model, which
260 is a normal, necessary assumption for head models with this level of complexity. One cannot
261 resort to computationally intensive fluid-structure interaction simulations, and this is usually
262 acceptable due to limited relative motion between the brain components. Furthermore, the
263 components in the current head model were unconstrained, except for the contact property
264 between them which restrained penetration. In reality, the various head components are
265 connected by different nerves, which restrict their relative motion to some extent. The
266 discretionary use of different types of contact interactions or constraints would affect the
267 simulation results, as also noted and reported by Bar-Kochba et al. (2012), but addressing this
268 issue is complex since there is limited in-vivo human head test data to reveal the actual contact
269 interaction properties between the various components.

Smaller regions of high ICPs and strains were observed in the brain during the impact as seen in Figure 5. When using a penalty contact formulation, penetration is avoided by upholding a restoring, coupling force between components. As for this relatively complex geometry of the brain and these large deformations, many local areas with high pressure can arise from these contact forces. This phenomenon was not reported by Milne et al. (2012) who employed a relatively simplified FE head model, in which the convoluted topography of the brain was idealised as a smooth surface.

## 4. Conclusion

In the current study, an enhanced, anatomically detailed and experimentally verified subject-specific head model, coupled with a bicycle helmet model was used to simulate the test impact as prescribed by the helmet standard EN 1078 for Europe, Asia, and South America. Using the simulation model, it was demonstrated how the peak resultant translational acceleration was reduced by 75%, the von Mises skull stress by 88%, the ICP by 31%, and the max. principal strain in the brain by 15% when the model was wearing a bicycle helmet in the test impact. It is anticipated that the presented numerical model can be used in the future to go beyond the enforced test standards in terms of evaluating and optimising helmet designs by analysing multiple and more complex injury scenarios.

***3609 words***

## Conflicts of interest

None

**Acknowledgments**

The first author would like to acknowledge the fruitful discussions and help he received from staff and students during his research stay at Applied Mechanics Laboratory, National University of Singapore.

**References**

Asiminei, A. G., Goffin, J., Van Der Perre, G., & Verpoest, I. (2009). A transient finite element study reveals the importance of the bicycle helmet material properties on head protection during an impact. *International Research Council on the Biomechanics of Injury - 2009 International IRCOBI Conference on the Biomechanics of Injury, Proceedings*, 357–360.

Bar-Kochba, E., Guttag, M., Sett, S., Franck, J. A., McNamara, K., Crisco, J.. & Franck, C. (2012). Finite Element Analysis of Head Impact in Contact Sports. In SIMULIA Community Conference (SCC) (p. 10).

Bicycle Helmet Safety Institute (2017). Bicycle Helmet Laws. Available at https://helmets.org/mandator.htm.

Cui, L., Kiernan, S., & Gilchrist, M. D. (2009). Designing the energy absorption capacity of functionally graded foam materials. *Materials Science and Engineering: A*, 507**(1)**, 215-225.

CPSC (1998), Consumer Product Safety Commission, Safety Standard for Bicycle Helmets; Final Rule, USA

Cripton, P. A., Dressler, D. M., Stuart, C. A., Dennison, C. R., & Richards, D. (2014). Bicycle helmets are highly effective at preventing head injury during head impact: Head-form accelerations and injury criteria for helmeted and unhelmeted impacts. *Accident Analysis & Prevention*, 70, 1-7.

Dassault Systmes (2013), ABAQUS User's Manual 6.13, Dassault Systmes, USA

315 European Commission (2011), The Gallup Organisation, Future of transport - Analytical
316 report, Europe
317 European Commission (2015). Road safety in the European Union; Trends, statistics and main
318 challenges, European Union
319 European Commission (2016) Road safety in the European Union; Trends, statistics and main
320 challenges, European Union
321 European standard (1997), EN 1078, Helmets for pedal cyclists and for users of skateboards
322 and roller skates
323 Kleiven, S., & Hardy, W. N. (2002). Correlation of an FE Model of the Human Head with
324 Local Brain Motion--Consequences for Injury Prediction. *Stapp Car Crash Journal*, (46),
325 123-44.
326 Fahlstedt, M., Halldin, P., & Kleiven, S. (2016). The protective effect of a helmet in three
327 bicycle accidents—A finite element study. Accident Analysis & Prevention, 91, 135-143.
328 Hardy WN, Foster C, Mason M, Yang K, King A, Tashman S. Investigation of head injury
329 mechanisms using neutral density technology and high-speed biplanar x-ray. *45th Stapp*
330 *Car Crash Conference*, San Antonio, USA, 2001; 337–368.
331 HEADS-ITN (2015*). Current Standards for Sports and Automotive Helmets: A Review.*,
332 Available at http://www.heads-itn.eu/pdfs/Helmets_Standard_Evaluation.pdf (Section
333 2.1)
334 ITF (2017). Road Safety Annual Report 2017, OECD Publishing, Paris.
335 McElhaney, J. H., Fogle, J. L., Melvin, J. W., Haynes, R. R., Roberts, V. L., & Alem, N. M.
336 (1970). Mechanical properties of cranial bone. *Journal of biomechanics*, 3**(5)**, 495-511.
337 McIntosh, A. S., Lai, A., & Schilter, E. (2013). Bicycle helmets: head impact dynamics in
338 helmeted and unhelmeted oblique impact tests. *Traffic injury prevention*, 14**(5)**, 501-508.

Morrison III, B., Cater, H. L., Wang, C. C., & Thomas, F. C. (2003). A tissue level tolerance criterion for living brain developed with an in vitro model of traumatic mechanical loading. *Stapp Car Crash Journal*, 47, 93.

Mills, N. J., & Gilchrist, A. (2008). Finite-element analysis of bicycle helmet oblique impacts. *International Journal of Impact Engineering*, 35**(9)**, 1087-1101.

Milne, G., Deck, C., Carreira, R. P., Allinne, Q., & Willinger, R. (2012). Development and validation of a bicycle helmet: Assessment of head injury risk under standard impact conditions. *Computer methods in biomechanics and biomedical engineering*, 15**(1)**, 309-310.

Milne, G., Deck, C., Bourdet, N., Carreira, R. P., Allinne, Q., Gallego, A., & Willinger, R. (2014). Bicycle helmet modelling and validation under linear and tangential impacts. *International Journal of Crashworthiness*, 19**(4)**, 323-333.

Nahum AM, Smith R, Ward CC. Intracranial pressure dynamics during head impact. *In 21st Stapp Car Crash Conference. Society of Automotive Engineers (SAE),* SAE Paper No. 770922: San Diego, USA, 1977; 339–366.

Newman, J. A., Shewchenko, N., & Welbourne, E. (2000). A proposed new biomechanical head injury assessment function-the maximum power index. *Stapp car crash journal*, 44, 215-247.

Olivier, J., & Creighton, P. (2016). Bicycle injuries and helmet use: a systematic review and meta-analysis. *International journal of epidemiology*, *46***(1)**, 278-292.

Schaller, A., Voigt, C., Huempfner-Hierl, H., Hemprich, A., & Hierl, T. (2012). Transient finite element analysis of a traumatic fracture of the zygomatic bone caused by a head collision. *International journal of oral and maxillofacial surgery*, 41**(1)**, 66-73.

Takhounts, E. G., Eppinger, R. H., Campbell, J. Q., & Tannous, R. E. (2003). On the development of the SIMon finite element head model. *Stapp car crash journal*, 47, 107.

364 Tan, L. B., Tse, K. M., Lee, H. P., Tan, V. B. C., & Lim, S. P. (2012). Performance of an
365 advanced combat helmet with different interior cushioning systems in ballistic impact:
366 Experiments and finite element simulations. *International Journal of Impact Engineering*,
367 50, 99-112.
368 Teng, T. L., Liang, C. L., & Nguyen, V. H. (2013). Development and validation of finite
369 element model of helmet impact test. Proceedings of the Institution of Mechanical
370 Engineers, *Part L: Journal of Materials Design and Applications*, 227**(1)**, 82-88.
371 Trosseille X, Tarriere C, Lavaste F. Development of a FEM of the human head according to a
372 specific test protocol. *In 30th Stapp Car Crash Conference. Society of Automotive*
373 *Engineers (SAE)*, SAE Paper No. 922527: Warrendale, USA, 1992; 235–253.
374 Tse, K. M., Tan, L. B. and Lee, H. P. (2017). Chapter 10: The Skull and Brain: Computer
375 models for the head and its protection. In Franklyn, M. and Lee, P. V. S. (eds) *Military*
376 *Injury Biomechanics: The Cause and Prevention of Impact Injuries*: CRC Press, pp. 175-
377 220.
378 Tse, K. M., Tan, L. B., Lim, S. P., & Lee, H. P. (2015). Conventional and complex modal
379 analyses of a finite element model of human head and neck. *Computer methods in*
380 *biomechanics and biomedical engineering*, 18**(9)**, 961-973.
381 Tse, K. M., Tan, L. B., Lee, S. J., Lim, S. P., & Lee, H. P. (2014). Development and validation
382 of two subject-specific finite element models of human head against three cadaveric
383 experiments. *International journal for numerical methods in biomedical engineering*,
384 30**(3)**, 397-415.
385 E. van den Bosch (2006), "Crash Helmet Testing and Design Specifications", Ph.D. thesis,
386 Eindhoven University of Technology, Department of Mechanical Engineering, Section of
387 Dynamics and Biomechanics.

388 Ward, C., Chan, M., & Nahum, A. (1980). Intracranial pressure–a brain injury criterion (No.
389 801304). SAE Technical Paper.
390 Willinger, R., Taleb, L., & Kopp, C. M. (1995). Modal and temporal analysis of head
391 mathematical models. *Journal of neurotrauma*, 12**(4)**, 743-754.
392 Zhang, L., Yang, K. H., & King, A. I. (2004). Comparison of brain responses between frontal
393 and lateral impacts by finite element modeling. *Journal of neurotrauma*, 18**(1)**, 21-30.
394

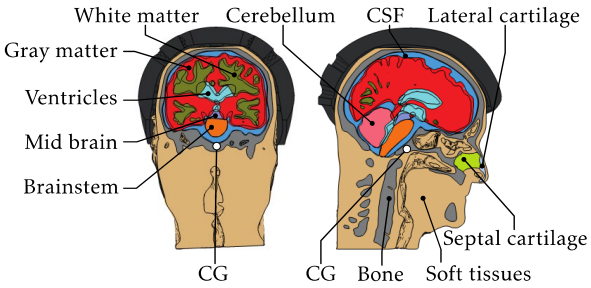


395

396 Figure 1: Frontal and sagittal view of head model, and probe location (CG).

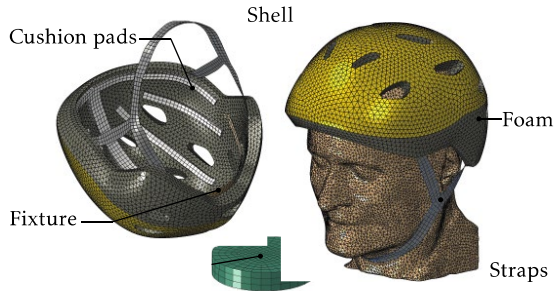


397

398 Figure 2: Mesh of bicycle helmet model, anvil and the assembled helmet-head model with
399 orientation of the coordinate system.

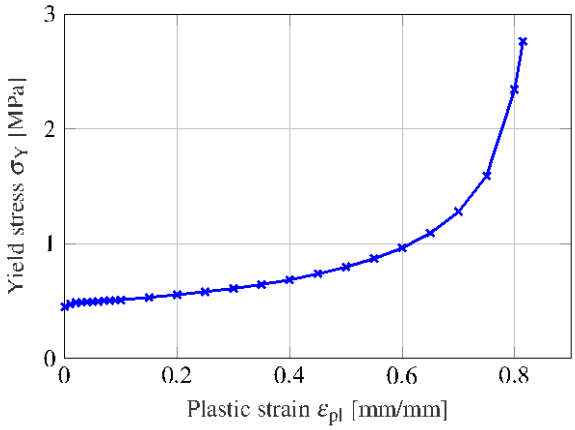


400

401 Figure 3: Constitutive relation (Yield stress/plastic strain) of the expanded polystyrene (EPS)
402 foam.

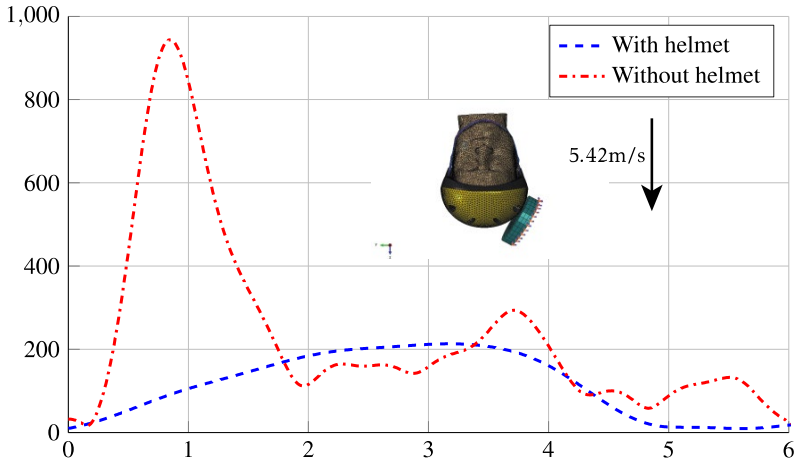


403

404 Figure 4: Resulting translational acceleration at CG of the headform for the EN 1078 impact,
405 equivalent to a 1.5 m guided free fall.

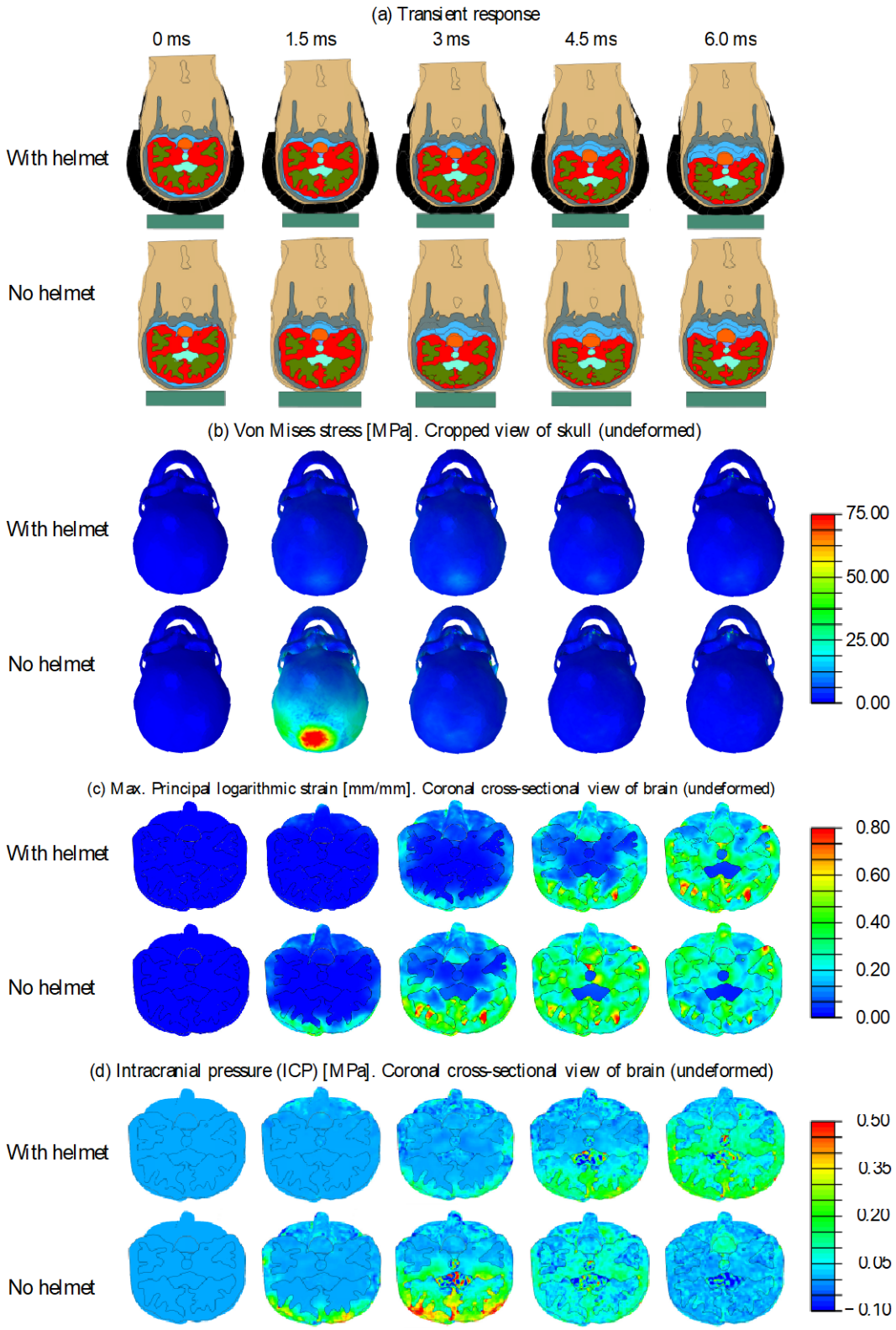


406

407 Figure 5: Resulting field variables for the EN 1078 impact: Guided 1.5 m direct free fall on
408 flat anvil. (a) Transient response, (b) Von mises stress, (c) Principal logarithmic strain, and
409 (d) Intracranial pressure.

410

| Components of the helmet | No. and types of elements* | Thickness [mm] | Elasticity [MPa] | Poisson's ratio [-] | Density [kg×mm$^{-3}$] | References |
|---|---|---|---|---|---|---|
| EPS Foam# | 48,416 C3D4 | 20 | E = 20; $\sigma_Y$ = 0.140; k = 0.1; $k_t$ = 1.933 | - | $0.064\times10^{-6}$ | Dassault Systmes (2013); Cui et al. (2009); Mills and Gilchrist (2008) |
| Cushion pads | 1,632 C3D4 | 3 | E = 0.47 | - | $0.032\times10^{-6}$ | Teng et al. (2013) |
| Shell | 4,116 S3R | 0.4 | E = 15 | 0.42 | $1.5\times10^{-6}$ | van den Bosch (2006) |
| Fixture | 128 S4R | 1.5 | E = 2 | 0.35 | $1.5\times10^{-6}$ | |
| Straps | 342 S4R | 1.5 | E = 0.06 | 0.25 | $0.4\times10^{-6}$ | Tan et al. (2012) |
| *Total, helmet: 54,000 elements, 0.194 kg* | | | | | | |
| **Components of the test setup** | **No. and types of elements*** | **Thickness [mm]** | **Elasticity [MPa]** | **Poisson's ratio [-]** | **Density [kg×mm$^{-3}$]** | **References** |
| Anvil | 576 C3D8R | 24 | $E$ =200 | 0.25 | $7.8\times10^{-6}$ | European standard (1997) |
| *Total, anvil: 576 elements, 2.32 kg* | | | | | | |
| **Components of the head** | **No. and types of elements*** | **Elasticity / Viscoelasticity [MPa]** $G(t) = G_\infty + (G_0 - G_\infty)e^{-\beta t}$ with $G_{0,\infty}$ [MPa], $\beta$ [$s^{-1}$]) | | **Poisson's ratio [-]** | **Density [kg×mm$^{-3}$]** | **References** |
| Brainstem^ | 6,104 C3D4 | $G_0$ = 0.0225, $G_\infty$ = 0.0045, $\beta$ = 80 | | 0.4996 | $1.06\times10^{-6}$ | Tse et al. (2014) |
| Cerebral peduncle^ | 1,762 C3D4 | $G_0$ = 0.0225, $G_\infty$ = 0.0045, $\beta$ = 80 | | 0.4996 | $1.06\times10^{-6}$ | Tse et al. (2014) |
| CSF | 164,864 C3D4 | $E$ = 1.314 | | 0.4999 | $1.04\times10^{-6}$ | Tse et al. (2014) |
| Grey matter^ | 436,917 C3D4 | $G_0$ = 0.034, $G_\infty$ = 0.0064, $\beta$ = 700 | | 0.4996 | $1.04\times10^{-6}$ | Tse et al. (2014) |
| Lateral cartilage | 2,874 C3D4 | $E$ = 30 | | 0.45 | $1.50\times10^{-6}$ | Tse et al. (2014) |
| Septum cartilage | 3,578 C3D4 | $E$ = 9 | | 0.32 | $1.50\times10^{-6}$ | Tse et al. (2014) |
| Bone | 130,482 C3D4 | $E$ = 8000 | | 0.22 | $1.21\times10^{-6}$ | Tse et al. (2014) |
| Soft tissues | 253,894 C3D4 | $E$ = 16.7 | | 0.46 | $1.04\times10^{-6}$ | Tse et al. (2014) |
| Ventricles | 36,776 C3D4 | $E$ = 1.314 | | 0.4999 | $1.04\times10^{-6}$ | Tse et al. (2014) |
| White matter^ | 278,925 C3D4 | $G_0$ = 0.034, $G_\infty$ = 0.0064, $\beta$ = 700 | | 0.4996 | $1.04\times10^{-6}$ | Tse et al. (2014) |
| *Total, head: 1,300,000 elements, 4.73 kg* | | | | | | |

# with material non-linearity, volumetric hardening

^ with material non-linearity, viscoelasticity, where $G_\infty$ is the long-term sheer modulus, $G_0$ is the short term sheer modulus, and $\beta$ is the decay factor

* C3D4 refers to solid tetrahedral and C3D8R refers to solid hexahedral elements. S3R and S4R are reduced-integration triangular and quadrilateral shell elements, respectively.

411

412 Table 1: Mechanical properties for the different components. If not otherwise stated,

413 components are considered isotropic and linear-elastic.

| Reference | Head model | Peak resultant linear acceleration | Impact duration |
|---|---|---|---|
| The current study | Tse et al. (2014), 4.73 kg | 223G | 5ms |
| Milne et al. (2012) | Strasbourg University Finite Element Head Model, 5.7 kg | 174G | 8ms |
| Fahlstedt et al. (2016) | Hybrid III dummy head, 4.54 kg | 220G | 6ms |

414

415 Table 2: Benchmarks for model validation.

| Field variable | Without helmet | With helmet | Reduction |
|---|---|---|---|
| Peak resultant linear acceleration | 944G | 223G | 75% |
| Von Mises stress in skull | 85 MPa (*1.2ms) | 10 MPa (3.6ms) | 88% |
| Max. Intracranial pressure (ICP) in brain | 0.65 MPa (3.4ms) | 0.45 MPa (5.3ms) | 31% |
| Max. Principal strain in brain | 0.8 [-] (3.4ms) | 0.7 [-] (5.4ms) | 15% |
| *(* all parentheses hold the time of the occurrence)* | | | |

416

417 Table 3: Peak values of acceleration and field variables, incl. reductions.